68th International Astronautical Congress (IAC), Adelaide, Australia, 25-29 September 2017.

IAC-17.A6.2.7

DYNAMICAL MAPPING OF THE LEO REGION FOR PASSIVE DISPOSAL DESIGN

E.M Alessi[a]*, G. Schettino[a], A. Rossi[a], G.B. Valsecchi[b]

[a] *IFAC-CNR, Via Madonna del Piano 10, 50019 Sesto Fiorentino (FI), Italy,* em.alessi@ifac.cnr.it, g.schettino@ifac.cnr.it, , a.rossi@ifac.cnr.it

[b] *IAPS-INAF, Via Fosso del Cavaliere 100, 00133 Rome, Italy,* giovanni@iaps.inaf.it

* Corresponding Author

Abstract

We present the results obtained within the H2020 ReDSHIFT project on the dynamical characterization of the Low Earth Orbit (LEO) region. An extended simulation campaign was performed in order to recognize the dynamical highways that can be exploited for the design of passive disposal strategies. The LEO region has been mapped in terms of semi-major axis, eccentricity, and inclination, by propagating for 120 years a grid of initial conditions including quasi-circular up to eccentric orbits, with semi-major axes up to 9400 km, prograde and retrograde inclinations, and 16 combinations of longitude of ascending node and argument of pericenter. For each set of initial conditions, two initial epochs and two values of area-to-mass ratio were considered. The outcome reveals the existence of resonant corridors due to lunisolar perturbations, geopotential zonal harmonics or solar radiation pressure, which can be used in combination with the atmospheric drag in order to achieve reentry. This information can be exploited, in the long-term simulations of the LEO environment, to devise optimal mitigation scenarios, minimizing the Delta V requirements to comply with a given residual lifetime of the spacecraft.

1. Introduction

In the framework of the ReDSHIFT (Revolutionary Design of Spacecraft through Holistic Integration of Future Technologies) H2020 project [1], a fundamental role is played by the will of achieving a deep understanding of the dynamics which governs the motion of the objects in the circumterrestrial space. Though the space era is 60 years old and very sophisticated operations can be performed in orbit around the Earth, still a full characterization of the orbital regimes is missing. Certainly, classical celestial mechanics tools and numerical methods have been applied so far to understand the main perturbations acting on Earth's orbits and their effects in the long- and short-term, but most of the studied focused on specific operational regions or initial conditions.

The main assumption of the astrodynamical analysis of the ReDSHIFT project is that the natural dynamics can help in the design of mitigation strategies for space debris. In particular, according to the orbital regime, the aim is to take advantage of highways directed naturally towards the reentry or a stable graveyard orbit. Such highways open up in correspondence of well-defined values of semi-major axis, eccentricity and inclination, due to the action of a given perturbation. The longitude of the ascending node, the argument of the pericenter and the epoch define, instead, where the highway is headed to.

To obtain a catalogue as accurate as possible of the possible location of these entrances, a numerical mapping was performed for Low Earth Orbits (LEO), Medium Earth Orbits (MEO) and Geostationary Earth Orbits (GEO). In this work, we discuss the main settings and results of the study done on LEO, and introduce some examples of how they can be useful for end-of-life strategies. The results obtained on MEO and GEO under the ReDSHIFT project can be found in [2] and [3], respectively.

2. Settings and Background

As detailed in [4, 5], the numerical simulation was done by propagating for an interval of 120 years a grid of initial conditions in semi-major axis a, eccentricity e and inclination i starting from 16 combinations of initial longitude of the ascending node Ω

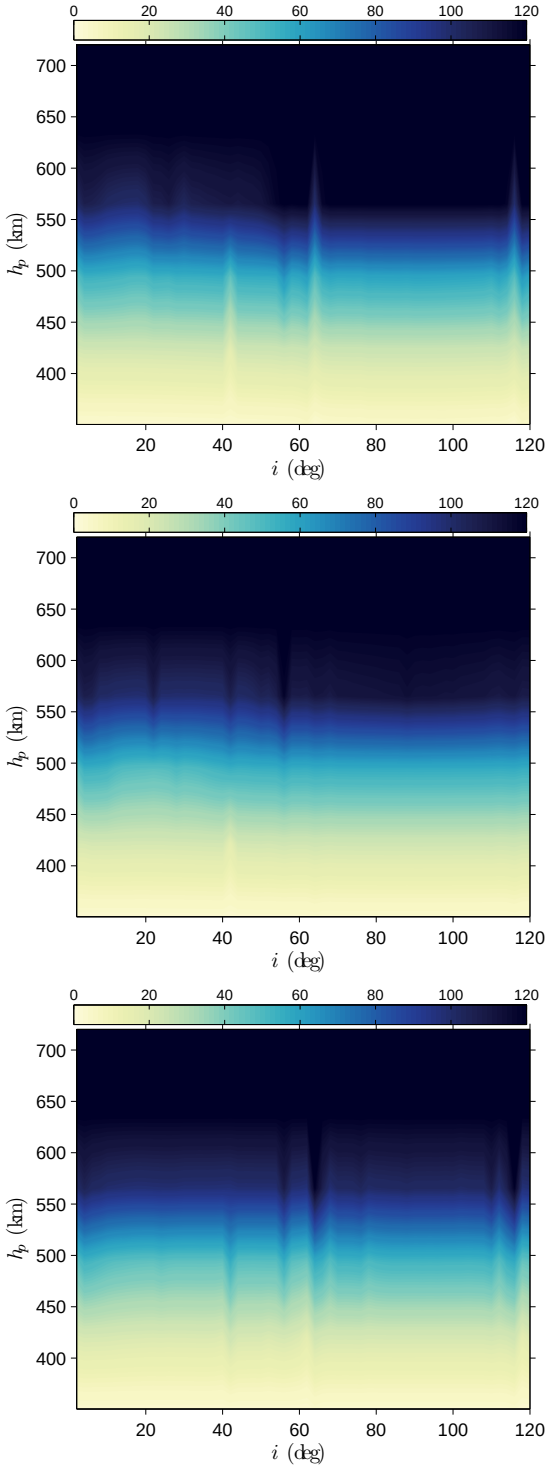

Figure 1: As a function of the initial inclination (deg) and pericenter altitude, the colorbar reports the lifetime (y), starting from $a = 780$ km $+ R_E$, the 2018 initial epoch and considering $A/m = 0.012$ m^2/kg. Top: $\Omega = 90°$, $\omega = 270°$. Middle: $\Omega = 180°$, $\omega = 0°$. Bottom: $\Omega = 270°$, $\omega = 180°$.

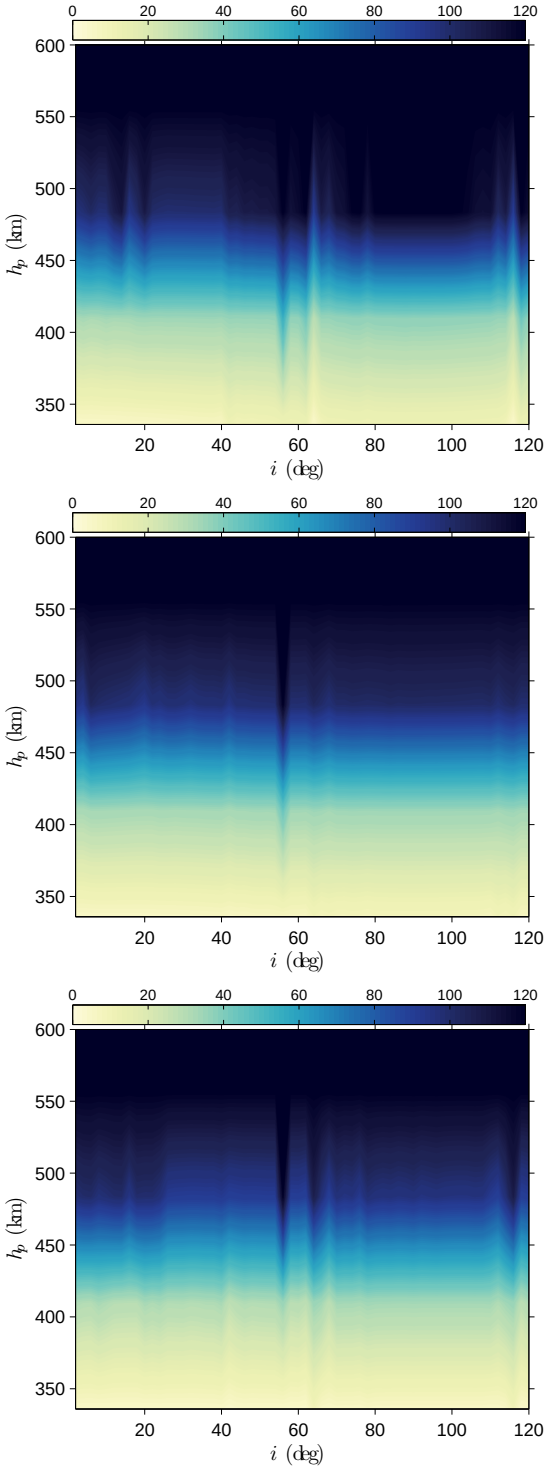

Figure 2: As a function of the initial inclination (deg) and pericenter altitude, the colorbar reports the lifetime (y), starting from $a = 1000$ km $+ R_E$, the 2018 initial epoch and considering $A/m = 0.012$ m^2/kg. Top: $\Omega = 90°$, $\omega = 270°$. Middle: $\Omega = 180°$, $\omega = 0°$. Bottom: $\Omega = 270°$, $\omega = 180°$.

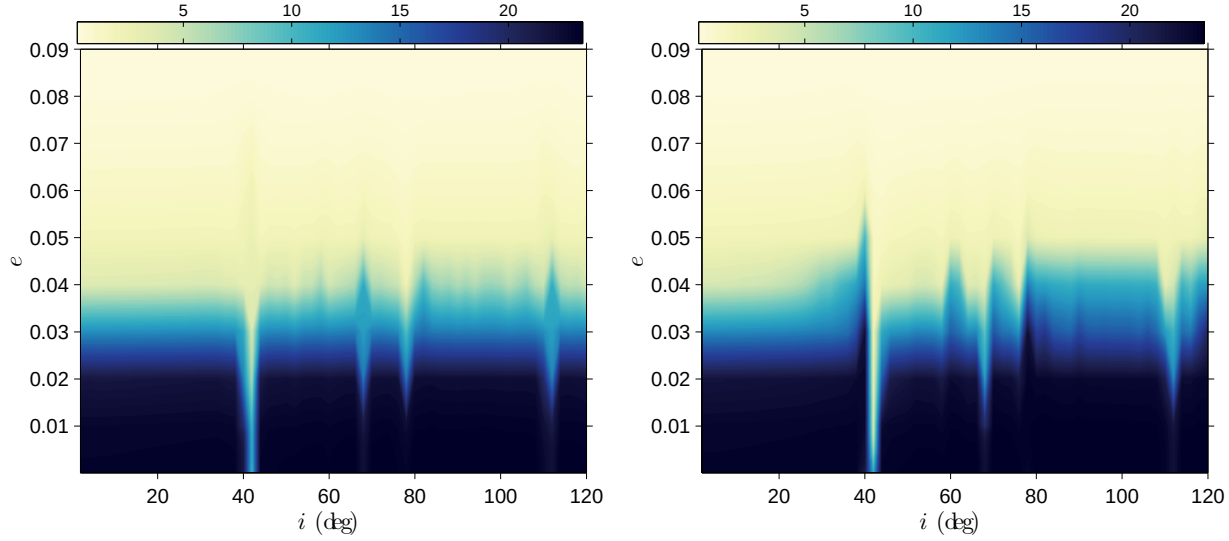

Figure 3: As a function of the initial inclination (deg) and eccentricity, the colorbar reports the lifetime (y), starting from $a = 1000$ km $+ R_E$, the 2020 initial epoch and considering $A/m = 1$ m^2/kg. Left: $\Omega = 0°$, $\omega = 0°$. Right: $\Omega = 90°$, $\omega = 270°$.

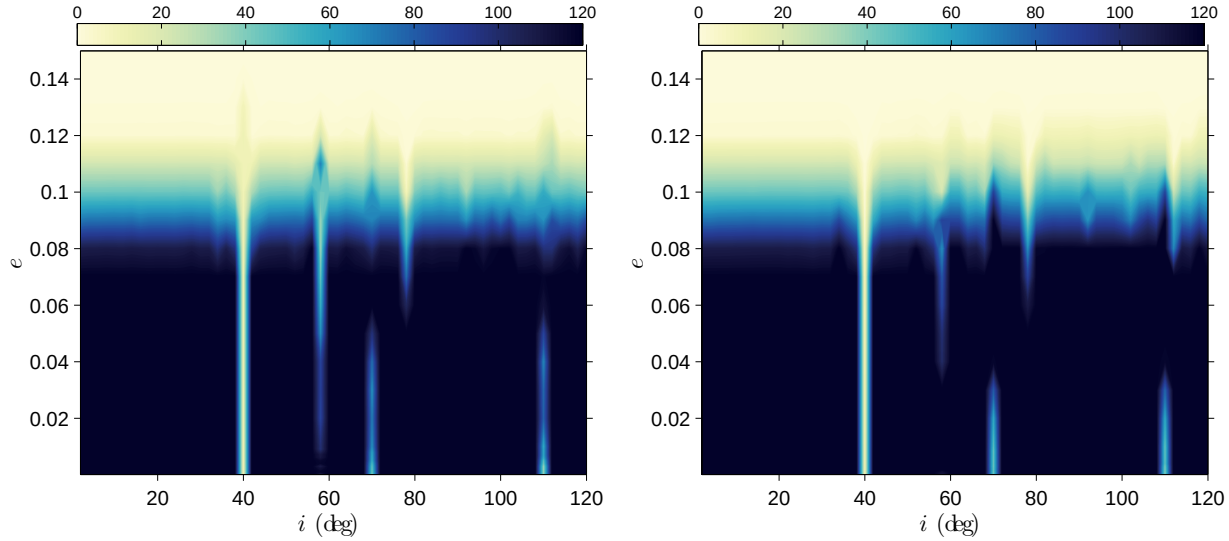

Figure 4: As a function of the initial inclination (deg) and eccentricity, the colorbar reports the lifetime (y), starting from $a = 1520$ km $+ R_E$, the 2020 initial epoch and considering $A/m = 1$ m^2/kg. Left: $\Omega = 0°$, $\omega = 0°$. Right: $\Omega = 90°$, $\omega = 90°$.

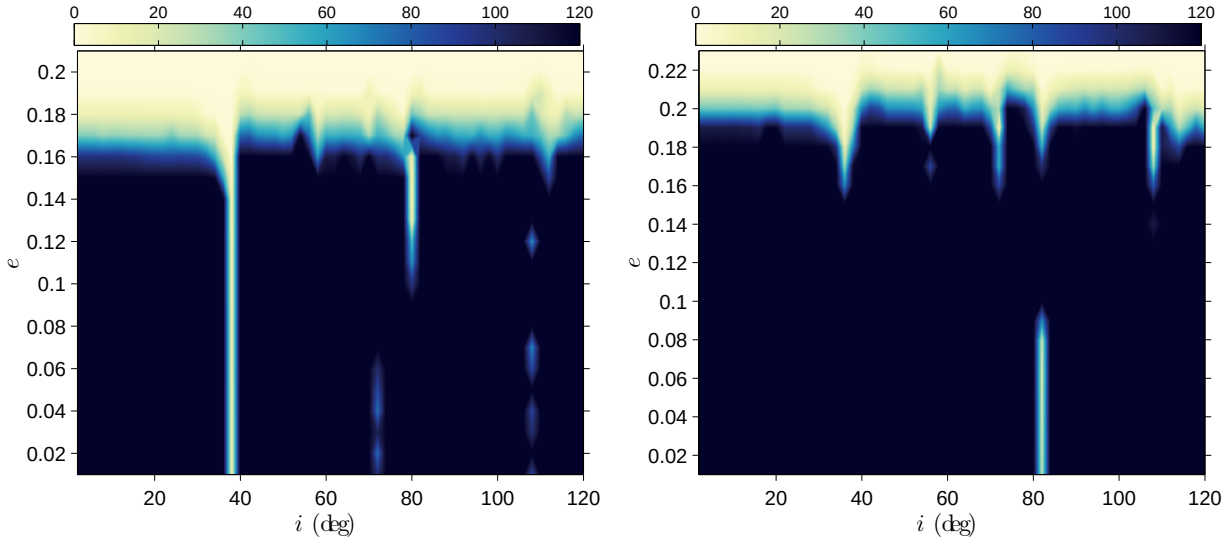

Figure 5: As a function of the initial inclination (deg) and eccentricity, the colorbar reports the lifetime (y), starting from $a = 2100$ km $+ R_E$, $\Omega = 0°$, $\omega = 90°$ (left), $a = 2400$ km $+ R_E$, $\Omega = 90°$, $\omega = 0°$ (right), the 2020 initial epoch and considering $A/m = 1$ m^2/kg.

and argument of pericenter ω, two different epochs ($t_0 = 22/12/2018$ and $t_0 = 21/6/2020$), and two values of area-to-mass ratio ($A/m = 0.012$ m^2/kg and $A/m = 1$ m^2/kg). The grid in semi-major axis covers the range $a \in [500 \text{ km} + R_E : 3000 \text{ km} + R_E]$, where R_E is the equatorial radius of the Earth, and the step size is defined as 20, 50 or 100 km, according to the region. In particular, for $a > 2000$ km $+ R_E$, $\Delta a = 100$ km; for $a \in [700 \text{ km} + R_E : 1000 \text{ km} + R_E]$ or $a \in [1300 \text{ km} + R_E : 1600 \text{ km} + R_E]$, $\Delta a = 20$ km; in all the other cases, $\Delta a = 50$ km. The eccentricity spans all possible values up to reentry (defined when the pericenter altitude is below 300 km), at a step of $\Delta e = 0.01$, except for $a < 1600$ km $+ R_E$ for which it was also adopted a finer grid with $\Delta e = 0.001$ up to $e = 0.01$. The values of inclination considered go up to $i = 120°$ at a step of $2°$.

The numerical propagator applied is FOP (Fast Orbit Propagator; see [6, 7]), which is an accurate, long-term orbit predictor, based on the LOP (Long-term Orbit Predictor; see [8]). The formulation is singly-averaged, non-singular in eccentricity, including the following contributions: geopotential up to degree and order 5; lunisolar perturbations; solar radiation pressure (SRP); atmospheric drag. The SRP model is the cannonball model, considering shadows; the atmospheric drag is applied for altitudes below 1500 km, assuming the drag coefficient $C_D = 2.1$, and using the Jacchia-Roberts density model with an exospheric temperature of 1000 K and a variable solar flux at 2800 MHz.

During the numerical integration, the algorithm checks if the orbit reenters, and save all the maximum and minimum values detected for a, e, i. As mentioned before, the objective of the simulation is to see where some perturbation can make the orbit unstable. In LEO, the emphasis is put in reducing the lifetime and helping the space operators to comply with the 25-year rule. It is well-known that, up to about 700 km of altitude for circular orbits, the atmospheric drag is effective to push a spacecraft towards a reentry, assuming a standard value of area-to-mass ratio. But what can yield other perturbation is partially known. In particular, the other perturbation which can provide a variation in semi-major axis in the long-term is the one due to the tesseral harmonics. The effect is, however, too small (by itself) to lower naturally the pericenter altitude. On the other hand, the other main perturbations can induce a variation in eccentricity, which also can be used to lower the pericenter altitude. The results are thus analyzed in the perspective of understanding the magnitude of the eccentricity increase, the regions where it can take place, and how it can be used.

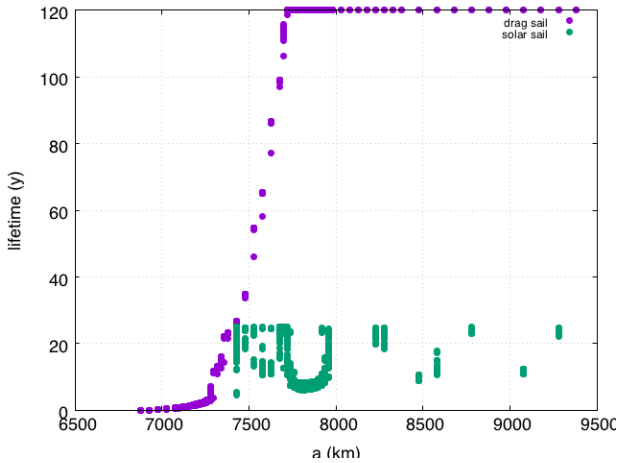

Figure 6: As a function of the initial semi-major axis (km), we show the lifetime (y) computed for orbits with an initial eccentricity up to 0.02, starting from the 2020 initial epoch and assuming $A/m = 1$ m^2/kg. In purple, the lifetime obtained considering only the action exerted by the atmospheric drag; in green, the lifetime computed considering the effect of the SRP. In the latter case, only the values complying with the 25-year rule are shown.

3. Cartography and Main Features

Given the amount of data obtained, the results are collected in a series of maps which depict the maximum eccentricity variation or the lifetime as a function of the initial inclination and initial eccentricity or initial pericenter altitude, for each combination of (t_0, a, Ω, ω). Some examples are given in Figures 1–2 and Figures 3–5 for the two values of area-to-mass ratio considered.

For $A/m = 0.012$ m^2/kg, which represents a standard value for intact objects, only the drag is able by itself to push the spacecraft towards the Earth, but this can happen only if the pericenter altitude is low enough, typically from about 580 km down to 350 km for increasing value of semi-major axis. Lunisolar perturbations, solar radiation pressure and zonal harmonics can speed up this process, but the variation they cause is not high enough to design a disposal strategy established only on their basis. In the examples shown, Figures 1–2, the colorbar reports the lifetime computed as a function of initial inclination and pericenter altitude starting from $a = 780$ km$+R_E$ and $a = 1000+$ km$+R_E$, the 2018 initial epoch, and three different orbital configurations. First, we can notice that in general, to comply with the 25-year rule, the eccentricity must be as high as about 0.043 for the first value of a, that is, the pericenter altitude lower than about 470 km. For the second value of a, the eccentricity must be at least about 0.08 in order to have a pericenter altitude lower than about 410 km. Similar considerations can be drawn for each value of semi-major axis simulated. Moreover, in each plot, we can also notice vertical stripes in correspondence of given values of inclination, which are 'yellower' or 'bluer' than the associated background, depending on the initial configuration. These are the 'entrances to the reentry highways', opened by lunisolar perturbation, high degree zonal harmonics or solar radiation pressure. Notice that a 'blue entrance' means that the lifetime increases, that is, the given perturbation acts against the action of the drag. Assuming that the drag acts in combination with a given different perturbation, if the lifetime increases, it means that the perturbation pushes the eccentricity towards a slight reduction, and thus the pericenter altitude will decrease in a slower way. Viceversa, if the perturbation contributes to a slight increase in eccentricity, it means that the reduction in pericenter altitude will be faster.

For $A/m = 1$ m^2/kg, the dynamics is different in the sense that the perturbation due to solar radiation pressure is able by itself to drive an object towards the Earth. This value of area-to-mass ratio can be considered as representative of a small spacecraft equipped with a sail, given the present technology. Looking to Figures 3–5, we can appreciate that the tenous stripes noticed for the lower value of area-to-mass ratio, stand out now in an evident way over the background. Note that they can induce a very significant reduction in lifetime also for circular orbits at very high values of semi-major axis (see Figure 5).

Up to altitudes of about 1050 km for circular orbits, the sail can be used as a drag sail to comply with the 25-year rule, starting from any value of initial inclination and (Ω, ω) configuration (see Figure 3). Beyond this value of altitude, if we consider only the action exerted by the drag, the lifetime increases exponentially, as expected. But for well-defined values of inclination, we can envisage the usage of the sail to exploit the solar radiation pressure effect. In Figure 6, we show the lifetime computed as a function of the initial semi-major axis starting from the initial epoch 2020 for values of initial eccentricity up to 0.02. In purple, we show the values obtained con-

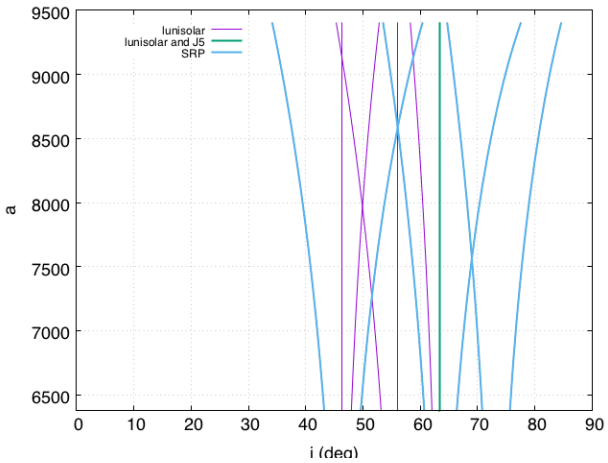

Figure 7: As a function of the initial inclination (deg) and semi-major axis (km), we show the location of the resonances found to play a role in the LEO region. The color of the curves describe the nature of the resonance. The curves have been computed for $e = 0.02$.

sidering only the action exerted by the atmospheric drag (within the assumptions on the solar flux detailed in Section 2.); in green, the values complying with the 25-year rule thanks to the SRP. Notice that this can be effective up to semi-major axis of about 9300 km, assuming the grid explored and the constraints set for the Figure.

3.1 Resonances

The inclination stripes evidenced in the previous Section can be explained in terms of orbital resonances, involving the variation of (Ω, ω) and the mean apparent motion of the Sun. For $A/m = 0.012$ m^2/kg, singly- and doubly-averaged lunisolar perturbation, 5th degree zonal harmonics and solar radiation pressure are the responsible of the relative significant variation in eccentricity, which was detected numerically. For $A/m = 1$ m^2/kg, solar radiation pressure resonances are the main effects to be considered. A detailed explanation on these mechanisms can be found in [4, 5, 9, 10]. In Figure 7, we show where they can be exploited, as a function of initial inclination and semi-major axis. The curves shown are computed assuming that both Ω and ω vary only because of the oblateness of the Earth, which is a good approximation in LEO for the two area-to-mass ratios considered. Note also that, for the values of eccentricity analyzed here, the location of the resonances is the one depicted in the Figure, i.e., a significant displacement of the curves associated with circular orbits or with relative high eccentric ones do not take place.

4. Disposal Strategies

The behavior revealed by the numerical simulation can be exploited for the design of end-of-life disposal strategies in two ways. Since an inclination-change maneuver is generally avoided due to the high cost (see Figure 8 for the circular case), a resonance shall be targeted only if the spacecraft is orbiting at an inclination value close enough to the resonant one, given semi-major axis and eccentricity. The information acquired can thus be used, far from a given resonance, in order to know which values of semi-major axis and eccentricity must be satisfied to ensure a reentry in 25 years. Certainly, the corresponding cost could be also too high. In Figure 9, we show these values for the grid explored, non-resonant values of inclination, and the two area-to-mass ratio assumed.

If instead the spacecraft is located at a resonance (or if the inclination-change maneuver is affordable), then the benefit can be considerable, especially if SRP effects are exploited. In Figure 10, we show the cost, in terms of Δv, computed assuming that the spacecraft is equipped with a sail, for an initial

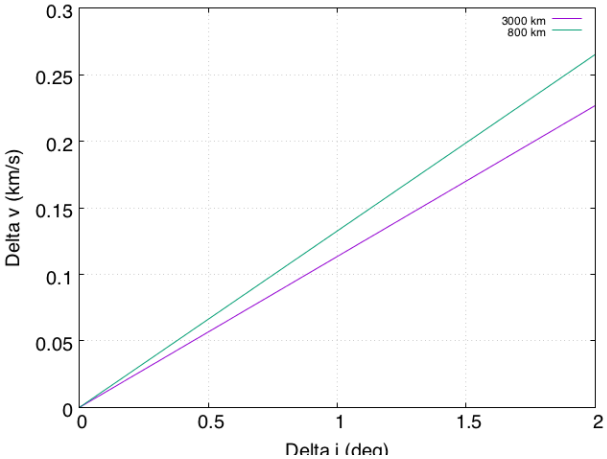

Figure 8: Cost (km/s) required to change the inclination (deg) of a circular orbit at two different altitudes: 800 km in purple, 3000 km in green, assuming that the maneuver is applied at the node.

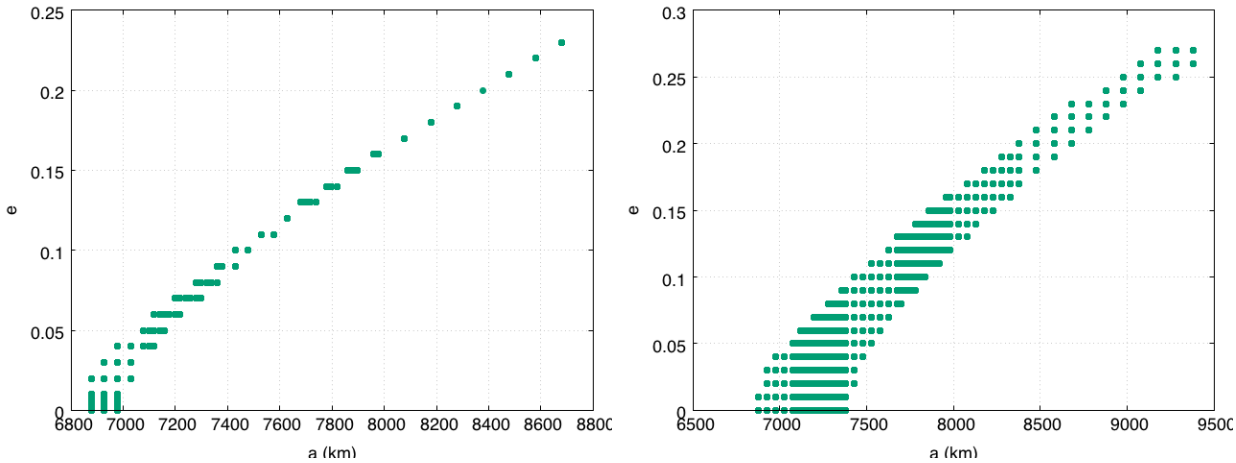

Figure 9: For $A/m = 0.012$ m^2/kg (left) and $A/m = 1$ m^2/kg (right), as a function of initial semi-major axis, the values of eccentricity ensuring a reentry in 25 years, for non-resonant values of inclination.

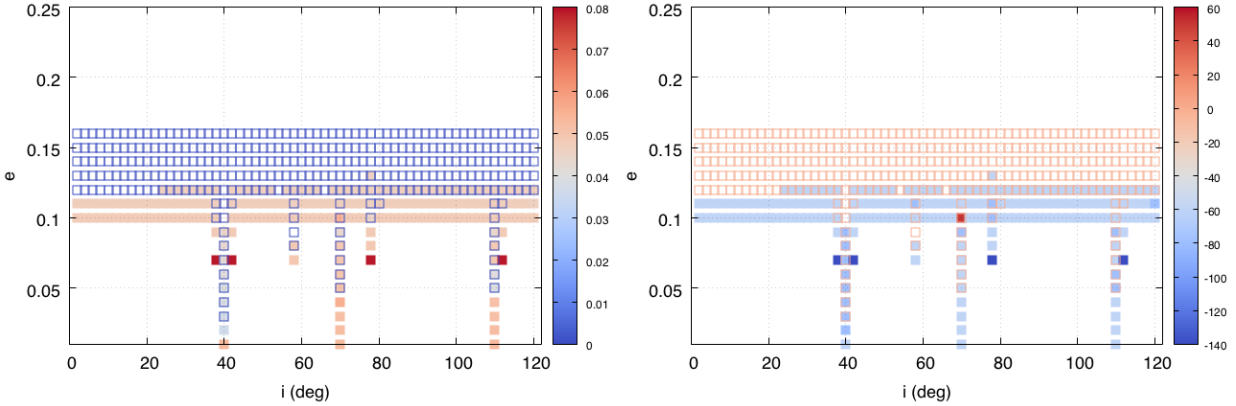

Figure 10: For $A/m = 1$ m^2/kg, as a function of initial (i, e) in the LEO region, examples of the 'minimum cost-reentry solutions' computed with a single-burn maneuver at the initial epoch 2020 for an initial semi-major axis equal to $a = 1600$ km $+ R_E$. The colorbar shows the Δv required (left), within a maximum threshold of 100 m/s, to reenter in 25 years. The empty squares represent solutions which do not need any impulsive maneuver. Left: cost (km/s). Right: Δa (km) targeted by the maneuver.

semi-major axis equal to $a = 1600$ km $+ R_E$. The empty blue squares in the Figure denote conditions which naturally reenter, because of the high value of area-to-mass ratio assumed. For values of eccentricity higher than 0.11, this is due to the effect of the drag, while for lower values of eccentricity, it is due to SRP. In the same Figure (left), full colored squares represent initial conditions which can take advantage of the SRP effect, after a maneuver lower than 100 m/s which aims at a slight different value of semi-major axis – the one shown in Figure 10 (right). Note that this example was obtained considering as targets the points simulated, that is, the grid described in Section 2.. Because the step size used in inclination was 2°, the procedure does not allow for a change in inclination, which would cost more than 100 m/s. For the possible implications on the usage of the sail, see [11].

5. Conclusions

In this work, we have given an overview of the main results obtained simulating the dynamics in the LEO region, considering a finite extended set of orbital elements, 120 years as maximum interval of time and two values of area-to-mass ratio. The possible exploitation of the data at our disposal covers a broad range of opportunities, which we have started to analyze. Here, we have mentioned the boundaries between atmospheric drag and solar radiation pressure, orbital resonances that can change significantly the long-term behavior, and end-of-life maneuvers that can be implemented on the basis of the outcome obtained. In the near future, special effort will be put in this direction, in order to compute the actual savings that resonant corridors can offer.

Acknowledgements

This work is funded through the European Commission Horizon 2020, Framework Programme for Research and Innovation (2014-2020), under the ReDSHIFT project (grant agreement n. 687500).

References

[1] A. Rossi and The ReDSHIFT team, The H2020 project ReDSHIFT: overview, first results and perspectives, in Proc. 7th European Conference of Space Debris, Darmstadt, Germany, 2017, 18-21 April, SDC7-521.

[2] D.K. Skoulidou, A.J. Rosengren, K. Tsiganis and G. Voyatzis, Cartographic study of the MEO phase space for passive debris removal, in Proc. 7th European Conference of Space Debris, Darmstadt, Germany, 2017, 18-21 April, SDC7-521.

[3] C. Colombo and I. Gkolias, Analysis of orbit stability in the geosynchronous region for end-of-ife disposal, in Proc. 7th European Conference of Space Debris, Darmstadt, Germany, 2017, 18-21 April.

[4] E.M. Alessi, G. Schettino, A. Rossi and G.B. Valsecchi, LEO mapping for passive dynamical disposal, in Proc. 7th European Conference of Space Debris, Darmstadt, Germany, 2017, 18-21 April, SDC7-508.

[5] E.M. Alessi, G. Schettino, A. Rossi and G.B. Valsecchi, Natural Highways for End-of-Life Solutions in the LEO Region, Cel. Mec. Dyn. Astron., (2017) submitted.

[6] L. Anselmo, A. Cordelli, P. Farinella, C. Pardini and A. Rossi, Study on long term evolution of Earth orbiting debris, ESA/ESOC contract No. 10034/92/D/IM(SC), 1996.

[7] A. Rossi, L. Anselmo, C. Pardini, R. Jehn and G.B. Valsecchi, The new space debris mitigation (SDM 4.0) long term evolution code, in Proc. of the Fifth European Conference on Space Debris, Darmstadt, Germany, 2009, 30 March-2 April, Vol. 672, id.90.

[8] J.H. Kwok, The long-term orbit prediction (LOP), JPL Technical Report EM 312/86-151, 1986.

[9] E.M. Alessi, G. Schettino, A. Rossi and G.B. Valsecchi, Solar Radiation Pressure Resonances in Low Earth Orbits, Mon. Not. R. Astron. Soc. (2017) submitted.

[10] G. Schettino, E.M. Alessi, A. Rossi and G.B. Valsecchi, Characterization of Low Earth Orbit Dynamics by Perturbation Frequency Analysis, in Proc. of the International Astronautical Congress, Adelaide, Australia, 25-29 September 2017, paper IAC-17.C1.9.2.

[11] C. Colombo, A. Rossi and F. Dalla Vedova, Drag and solar sail deorbiting: re-entry time versus cumulative collision probability, in Proc. of the International Astronautical Congress, Adelaide, Australia, 25-29 September 2017, paper IAC-17.A6.2.8.